Lawrence Berkeley National Laboratory

Title
Photoionization and photofragmentation of singly charged positive and negative Sc3N@C80 endohedral fullerene ions

Permalink
https://escholarship.org/uc/item/0b15m4tn

Journal
Physical Review A, 99(6)

ISSN
2469-9926

Authors
Müller, A
Martins, M
Kilcoyne, ALD
et al.

Publication Date
2019-06-01

DOI
10.1103/physreva.99.063401

Peer reviewed

Photoionization and photofragmentation of singly charged positive and negative Sc₃N@C₈₀ endohedral fullerene ions

A. Müller,[1,][*] M. Martins,[2] A. L. D. Kilcoyne,[3] R. A. Phaneuf,[4] J. Hellhund,[1] A. Borovik Jr.,[5] K. Holste,[5] S. Bari,[6]
T. Buhr,[5] S. Klumpp,[6] A. Perry-Sassmannshausen,[5] S. Reinwardt,[2] S. Ricz,[7] K. Schubert,[6] and S. Schippers[5]

[1]*Institut für Atom- und Molekülphysik, Justus-Liebig-Universität Gießen,*
Leihgesterner Weg 217, 35392 Giessen, Germany
[2]*Institut für Experimentalphysik, Universität Hamburg,*
Luruper Chaussee 149, 22761 Hamburg, Germany
[3]*Advanced Light Source, Lawrence Berkeley National Laboratory,*
1 Cyclotron Road, M.S. 7R0222, Berkeley, CA 94720-8229, USA
[4]*Department of Physics, University of Nevada, Reno, NV 89557-0058, USA*
[5]*I. Physikalisches Institut, Justus-Liebig-Universität Gießen,*
Heinrich-Buff-Ring 16, 35392 Giessen, Germany
[6]*Deutsches Elektronen-Synchrotron DESY, Notkestr. 85, 22607 Hamburg, Germany*
[7]*Institute for Nuclear Research, Hungarian Academy of Sciences, P.O. Box 51, 4001 Debrecen, Hungary*
(Dated: April 6, 2019)

Photoprocesses of the endohedral fullerene ions Sc₃N@C₈₀⁺ and Sc₃N@C₈₀⁻ in the gas phase have been investigated in the photon energy ranges 30 - 50 eV and 280 - 420 eV. Single and double ionization as well as single ionization accompanied by the release of a C₂ dimer were observed as a function of the photon energy for the positive parent ion and double detachment was measured for the negative parent ion. The emphasis of the experiments was on the specific effects of the encapsulated trimetallic nitride cluster Sc₃N on the observed reactions. Clear evidence of photoexcitation near the Sc *L* edge is obtained with the dominating contributions visible in the one- and two-electron-removal channels. *K*-vacancy production in the encapsulated central nitrogen atom is seen in the single ionization of Sc₃N@C₈₀⁺ but is much less pronounced in the photoionization-with-fragmentation channel. Comparison of the cross sections near the carbon *K* edge with the corresponding channels measured previously in the photoionization of Lu₃N@C₈₀⁺ reveal strong similarities. Previously predicted sharp resonance features in the ionization of Sc₃N@C₈₀⁺ ions below the Sc *M* edge are not confirmed. The experiments are accompanied by quantum-chemistry calculations in the Hartree-Fock approximation and by model calculations employing density functional theory (DFT).

I. INTRODUCTION

The first experimental evidence for the existence of soccer-ball-shaped C₆₀ molecules [1] initiated an immensely growing activity in several different fields of science. Almost in parallel with the exploration of the new class of spherical carbon structures, it was speculated and then realized that the carbon spheres can host and isolate single atoms or molecules and even clusters of atoms that can only be stabilized inside a spherical or nearly spherical carbon shell [2, 3]. Research on such carbon cages with encapsulated atoms, i.e., endohedral fullerenes, was spurred by scientific interest in the behavior of these intriguing nanoscale objects and by the perspectives of their usefulness in many diverse fields of applications ranging from medical treatment to the development of efficient solar cells and the realization of qubits in a spin quantum computer. All these aspects have been reviewed many times. Here, only a few references to recent reviews on endohedral fullerenes are provided [4–6].

One research direction among the wide and diverse scientific endeavours aiming at the detailed understanding of the nature and applicability of fullerenes and endohedral fullerenes is associated with their response to electromagnetic radiation [7–10]. The references given in recent publications [11–15] provide an overview of experimental research in the field of photoionization and photofragmentation of fullerenes. Investigating many-particle systems such as molecules, clusters and fullerenes by observing fine structure near atomic inner-shell photoabsorption edges is particularly elucidating. Examples of measurements employing gas-phase near-edge x-ray absorption fine structure (NEXAFS) spectroscopy of nanoparticles, biopolymers, and ionic species have been provided in a recent overview article [16].

Most of the work on photoprocesses involving fullerenes and endohedral fullerenes is theoretical ([8, 17] and references therein) because experiments are hampered by the limited availability of pure fullerene samples. The problem of sample purity can be overcome by employing mass-selective preparation of fullerene targets. This is possible by producing beams of electrically charged fullerenes and passing them through mass-over-charge filters. When beams of fullerene ions are made to interact with photon beams for studying photoionization and photofragmentation, the advantage of pure-target preparation is accompanied by the possibility of measuring absolute cross sections [10]. During the
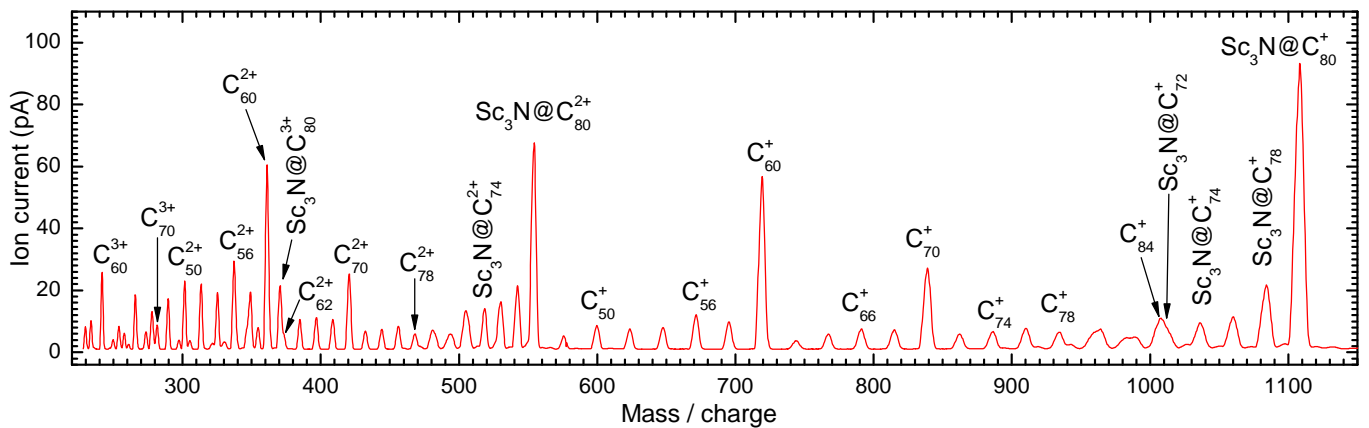
* Alfred.Mueller@iamp.physik.uni-giessen.de

FIG. 1. (color online) Magnetically analyzed mass-per-charge spectrum of positive ions extracted from an ECR ion source while evaporating a $Sc_3N@C_{80}$-containing fullerene sample into the plasma chamber of the source.

last one and a half decades, photon-ion merged-beams experiments were carried out with positively and negatively charged fullerene ions [13, 14, 18–20] and with positively charged endohedral fullerenes $Sc_3N@C_{80}^+$ [21], $Ce@C_{82}^+$ [22], $Xe@C_{60}^+$ [23, 24] and $Lu_3N@C_{80}^+$ [15].

The focus of this communication is on gas-phase experiments with $Sc_3N@C_{80}^q$ in charge states $q = \pm 1$. A wide range of photon energies is covered which include the regions of Sc M-shell and L-shell absorption edges as well as the K edges of C and N. Previous experimental studies of photoprocesses involving the Sc L edge together with the N K and the C K edges in neutral $Sc_3N@C_{80}$ comprise the observation of photo-electrons [25], of photoabsorption [26, 27], of core-level photoemission [26] and of momentum-resolved multi-coincidence spectra [12]. Pioneering work on $Sc_3N@C_{80}^+$ ions [21] investigated the influence of the Sc_3N cluster on the photoionization of the $Sc_3N@C_{80}^+$ parent ions in the energy range of approximately 30 to 50 eV. The latter experiment stimulated theoretical work on photoionization of $Sc_3N@C_{80}^+$ ions [28, 29] in which excess cross sections were arising from the encapsulated atoms compared to the cross section for the C_{80} carbon shell. A particularly intriguing prediction was made by Korol and Solov'yov [28] of narrow autoionizing Sc excitation resonances in the photoionization of $Sc_3N@C_{80}^+$ ions. This prediction provided part of the motivation for the present experimental investigation.

The present paper is organized as follows. The experimental arrangements and procedures are described in Sec. II. Sec. III briefly explains the theoretical approaches employed to calculate the geometry, electron distribution and the photoabsorption of the endohedral fullerene $Sc_3N@C_{80}$ in different initial charge states. The results of model calculations and experiments are presented and discussed in Sec. IV. The paper ends with a summary.

II. EXPERIMENT

The experiments were carried out at two different synchrotron-radiation sources during several beam-time periods at each of the facilities. The photon-ion merged-beams technique [10] was employed both at the Advanced Light Source (ALS) in Berkeley and at PETRA III in Hamburg. Two permanent experimental installations were used, namely, the PIPE (Photon-Ion Spectrometer at PETRA III) endstation [30, 31] of beamline P04 [32] and the IPB (Ion-Photon Beamline) endstation [33] of beamline 10.0.1. at the ALS. Several of the most recent publications of the present collaboration on photoprocesses of ions studied at the endstations at the ALS [13, 34–37] and at PETRA III [38–43] illustrate the experimental capabilities and the latest developments.

The basic concepts of the endstations used for the present experiments are very similar. The desired ions are produced by a suitable ion source. The extracted ions are accelerated by a voltage of 6 kV. The ion beam is dispersed in a magnetic field and ions of a given mass and charge are selected for further transportation to the photon-ion merged-beams region. Product ions are separated from the parent ion beam by a second magnet and directed to a single-particle detector. The observed detector count rates are normalized to the measured photon and parent-ion fluxes to obtain product yields. There is also the possibility to measure absolute cross sections by characterizing the overlap of the two interacting beams. However, beam-overlap form factors [10] were obtained only at the time when the single-ionization channel of $Sc_3N@C_{80}^+$ was measured in the photon-energy range 30 to 50 eV where Sc M-shell excitation may occur. In all other experiments discussed in the present context, only relative yields were recorded as a function of the photon energy. Cross sections with relatively large uncertainties estimated to be of the order of 50% are obtained for $Sc_3N@C_{80}^+$ ions by normalization to absorption cross sections prescribed by Henke *et al.* [44] for a molecule or
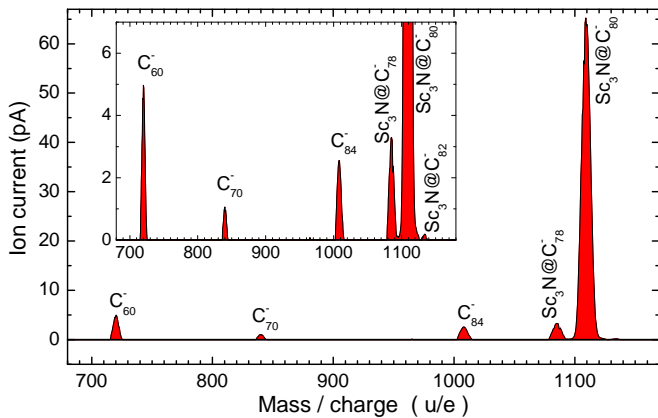
FIG. 2. (color online) Magnetically analyzed mass-per-charge spectrum of negative ions extracted from the ECR ion source while evaporating a $Sc_3N@C_{80}$-containing fullerene sample into the plasma chamber of the source.
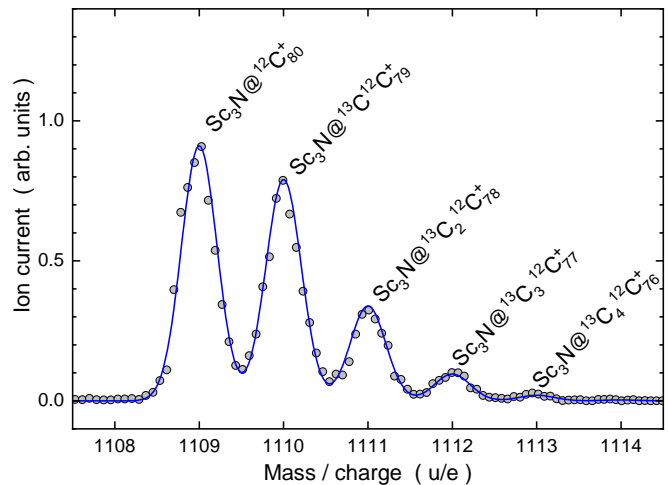

FIG. 3. (color online) High-resolution mass spectrum of $Sc_3N@C_{80}^+$ ions. Isotopologues containing different numbers of ^{13}C atoms are resolved. The solid line follows from combinatorial statistics when considering the natural abundances of the carbon isotopes.

cluster consisting of 80 C atoms, 3 Sc atoms, and 1 N atom. In the case of $Sc_3N@C_{80}^-$ parent ions, a typical beam overlap factor was assumed to estimate the absolute cross section. Considering the observed variations of beam overlaps, an uncertainty of a factor of 2 is assessed in that case.

In both endstations, the identical type of single-particle detectorwas used that has a high detection efficiency and very low dark-count rate. Atomic ions are detected with almost 100% efficiency while the very heavy fullerene ions may be detected with only 50 to 70% efficiency depending on their velocity. For the production of positive and negative $Sc_3N@C_{80}$ ions at the two endstations, two identical versions of a 10-GHz electron-cyclotron resonance (ECR) ion sourcewere employed.

Mass-per-charge spectra of $Sc_3N@C_{80}^+$ and $Sc_3N@C_{80}^-$ ions are shown in Fig. 1 and Fig. 2, respectively. Powder samples of heavy fullerenes with 20% enriched $Sc_3N@C_{80}$ were evaporated in an oven inside the plasma chamber of the ECR ion source. In both cases, minimal radio-frequency power (< 1 W) was applied to support the plasma discharge. However, the spectra are very different. The positive-ion spectrum is rich and shows numerous different fullerene ions. The samples contained fractions of C_{60}, C_{70}, C_{84}, and $Sc_3N@C_{80}$ which can be directly ionized in the source plasma. Singly, doubly and triply charged ions of these fractions are visible in the positive-ion spectrum Fig. 1. In addition, numerous other ion species are produced by fragmentation of the original fullerenes of the powder sample in the source plasma. Only fragments with even numbers of carbon atoms are produced.

In contrast to the positive-ion production, the spectrum of negative ions shows only a few species, predominantly the negative ions of the fullerenes contained in the sample powder. Two additional peaks are observed in the negative-ion spectrum shown in Fig. 2, the anion of $Sc_3N@C_{78}$ which is probably a product of ionization with fragmentation, and the anion of $Sc_3N@C_{82}$ which is suspected to be initially present in the original sample powder. The relative lack of fragmentation products in the negative-ion spectrum might be explained by a very low electron temperature in the ECR plasma providing optimum conditions for negative-ion production by electron attachment while suppressing fragmentation. It is also possible that fragment anions are much less stable than the parent anions and do not survive the flight times in the apparatus.

The mass resolving power $m/\Delta m$ in the spectra shown in Fig. 1 and Fig. 2 is of the order of 100. By closing the entrance and exit slits of the analyzer magnet much better resolution can be achieved. Figure 3 shows the mass-per-charge peak of $Sc_3N@C_{80}^+$ at a resolving power of 2240. Under this condition, the peak is resolved revealing five different contributions. The dominant peak at mass number 1109 is associated with the endohedral fullerene containing 80 ^{12}C atoms, the peak at mass number 1110 belongs to endohedral fullerenes containing 79 ^{12}C atoms and 1 ^{13}C atom. The mass number of an endohedral fullerene increases with the constituent number of ^{13}C atoms. Assuming that the endohedral fullerene material was synthesized using carbon with its natural abundances of isotopes one can calculate the mass distribution function on the basis of combinatorial (binomial) probabilities. The solid line in Fig. 3 represents the resulting distribution expected at a mass resolving power of 2240, in excellent agreement with the measured mass spectrum.

The measurement at high mass resolution demonstrates the purity of the primary $Sc_3N@C_{80}^+$ ion beam. Contaminations with other ions of identical mass-per-charge ratio can be excluded. High resolution requires the closing of slits and, hence, reduction of transmitted

ion current. Therefore, the photo-product spectra were recorded at moderate mass resolution with $m/\Delta m \approx 100$ to maximize the ion current.

The photon energy in the rest frame of the ions depends on the settings of the beamline optics and the velocity of the ions in the laboratory frame. At an energy of 6 keV, the $Sc_3N@C_{80}^+$ parent ions have a velocity of 3.23×10^6 cm/s which is about 0.01% of the vacuum speed of light. At low photon energies in the range of 30 to 50 eV the Doppler effect in the counter-propagating photon and ion beams is only a few meV. Calibration errors of the beamline at the ALS in this low-energy regime are no more than 20 meV. No special effort was made to determine the photon energy in this range with better accuracy.

For the measurements with $Sc_3N@C_{80}^+$ ions at energies in the range 280 to 320 eV at the ALS the photon energy was calibrated to the $\pi*$ resonance of the CO_2 molecule [45, 46]. At PIPE, the energy range covered in the experiments was $280 - 420$ eV. For the measurements with $Sc_3N@C_{80}^+$ ions the photon energy was calibrated to the dominant $1s \rightarrow 2p$ resonances in the photoionization of C^+ [41] and of Ne^+ [31]. For the combined spectra resulting from the measurements with $Sc_3N@C_{80}^+$ ions at the ALS and at PETRA III the uncertainty of the energy scale in the range 280 - 420 eV is estimated to be 0.2 eV. In the separate run with $Sc_3N@C_{80}^-$ ions the photon energy was calibrated to resonances in neutral O_2 [47] and Ne [31, 48]. The resulting uncertainty of the photon energies in the range 280 - 420 eV is estimated to be 0.3 eV.

III. MODEL CALCULATIONS

Model calculations in support of the experiments have been carried out for $Sc_3N@C_{80}^{q+}$ fullerenes for initial charge states $q = -1, 0, +1, +2, +3,$ and $+4$. The initial geometry of the fullerene ions as well as the distribution of electrical charges among the atomic constituents was determined as a function of q. NEXAFS spectra were calculated on a relative cross-section scale using approaches of density functional theory (DFT; a recent review of DFT and a discussion of the most commonly used density functionals has been provided by Mardirossian and Head-Gordon [49]). The model specifically includes photoabsorption at the K edge of nitrogen and the L edge of scandium. For the calculations it was assumed that the production process of the fullerene sample used for the experiments favored the formation of $Sc_3N@C_{80}$ with I_h symmetry [25].

The geometry of the endohedral fullerenes with charge states from -1 to +4 was optimized by quantum-chemistry calculations using the GAMESS package [50] in the Hartree-Fock approximation employing a 6-31G** basis set. As the starting geometry, the I_h (31924) symmetry of the $Sc_3N@C_{80}$ fullerene calculated by Popov and Dunsch [51] was chosen. From the optimization, the positions and electrical charges were obtained for the different atoms constituting the $Sc_3N@C_{80}^{q+}$ ($q = -1, ..., +4$) fullerene molecules.

The photoabsorption spectra were calculated using the StoBe code [52] on the DFT level employing Becke88 and Perdew86 functionals [53, 54] for the exchange and correlation terms, respectively. For a proper description of the photo-excited orbitals, additional auxiliary basis sets A2-DZVP (4,3;4,3) were added for the carbon and nitrogen atoms and A2-DZVP (5,5;5,5) for the scandium atoms. These basis sets are described by Godbout *et al.* [55]. The calculations of the x-ray absorption are based on the transition-state approach described by Triguero *et al.* [56]. For the Sc $2p$ excitation all orbitals below the $2p$ subshell were frozen during the calculation. Furthermore, the $2p$ orbitals of the two unexcited Sc atoms as well as the N $1s$ orbital were frozen considering the near degeneracy of the Sc $2p$ and N $1s$ electrons. During the N $1s$ NEXAFS calculation all Sc $2p$ orbitals were frozen. Since spin-orbit splitting is not included in the StoBe code, it has been artificially added for the Sc $2p$ excitation by splitting the calculated spectra into two components separated by 4.9 eV according to the atomic spin-orbit splitting [57]. The statistical branching ratio for the L_3 and L_2 excitations would be expected to be 2:1, however, in photoionization of the Sc atom [57] and the Sc^+ ion [58] a ratio close to 1:1 is found, which is also applied here. For simplicity the resonance positions were taken from the transition-state-approach computations and no additional calculation for the fully relaxed core hole states was performed.

The StoBe code only provides osillator strengths for individual transitions at given resonance energies. For a realistic description of photoabsorption the widths of the excited atomic and molecular levels have to be suitably modeled. For this purpose, the widths of the N K- and Sc L-shell resonance contributions were assumed to be 0.5 eV at energies up to 410 and 415 eV, respectively, where the excited levels preferentially decay via an Auger process. At higher photon energies the excited levels acquire shape-resonance character suggesting a considerably larger width. For energies beyond 420 eV for the N atom and 425 eV for the Sc atoms, widths of 4 eV were assumed. In the energy ranges 410 to 420 eV for N and 415 to 425 eV for Sc a linear increase of the widths as a function of photon energy was applied.

IV. RESULTS

A. Model-based findings

The treatment of the $Sc_3N@C_{80}^{q+}$ molecule in different charge states q by employing the GAMESS package [50] in the Hartree-Fock approximation yielded the electrical charges of the C, N, and Sc atoms as well as their radial distances from the center of the molecule. The results of the present model calculations are shown as a function of the charge state q in Fig. 4 a) and b), respec-
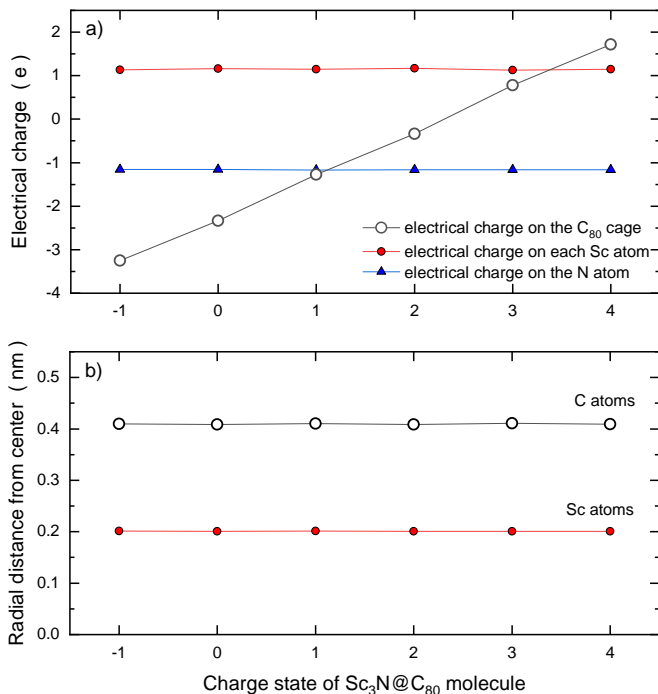
FIG. 4. (color online) Electrical charges (a) and radial distances (b) of the atoms in the $Sc_3N@C_{80}^{q+}$ molecule in different charge states q resulting from the present model calculations. The charges on the different atoms were obtained from a Mulliken analysis [59].
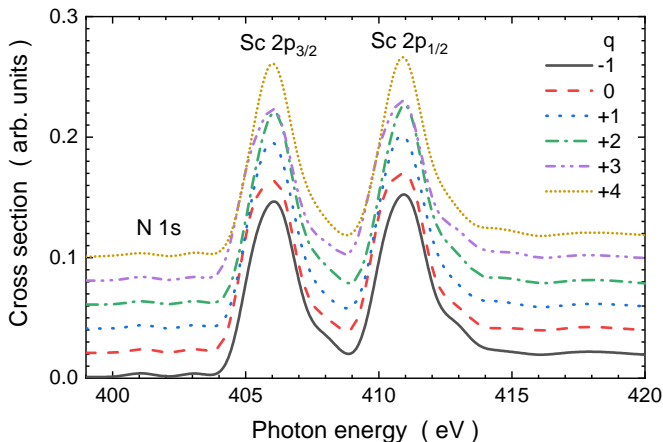

FIG. 5. (color online) Relative photoabsorption cross sections of the $Sc_3N@C_{80}^{q+}$ molecule in different charge states q resulting from the present model calculations. The results for charge states $q+1$ are vertically offset from those of q by 0.02 units ($q = -1, 0, +1, +2, +3$).

tively. The charges of the encapsulated N and Sc atoms obtained by a Mulliken population analysis [59] do not change when the whole endohedral molecule carries different charges (see Fig. 4 a). As one goes from $q = -1$ up to $q = +4$, electrons are practically only taken from the cage although the carbon sphere is known to have a large electron affinity. A Löwdin population analysis [60]

for the charge of the individual atoms shows the same trend with q. It is less surprising then that the geometry of the $Sc_3N@C_{80}^{q+}$ molecule does not significantly change with the charge state q. The nitrogen atom is known to reside approximately in the center of the endohedral molecule [25]. This is also found in the present treatment. The three scandium atoms form an equilateral triangle with the nitrogen atom in the center and, hence, all atoms of the Sc_3N cluster are located in one plane. According to the present model calculations, the Sc atoms have a radial distance of 0.20 nm from the center of the $Sc_3N@C_{80}^{q+}$ molecule independent of the charge state q. Such independence is also found for the carbon atoms of the cage with an average distance of 0.41 nm from the central N atom. For neutral $Sc_3N@C_{80}$ with I_h symmetry, the corresponding distances provided by Popov and Dunsch are 0.203 nm and 0.412 nm [51], respectively, in excellent agreement with the present findings. Most important in the present context was that neither the geometry nor the distribution of electrical charges significantly depend on the charge state q, at least for the sequence $q = -1, 0, +1, +2, +3, +4$.

From the results reported in the preceding paragraph, with the geometry of the endofullerene and the electrical charges on the scandium and nitrogen atoms not changing when the charge state q of the initial $Sc_3N@C_{80}^{q+}$ molecule is varied, one may also expect that the cross section for photoabsorption by the encapsulated Sc_3N cluster does not strongly depend on q. This expectation is confirmed by Fig. 5 which shows the results of the present model calculations using the StoBe code [52] on the DFT level described in Sec. III. Indeed, the sizes and spectral shapes of the (relative) cross sections obtained for different charge states q are very similar. In particular, the peak energies are found to be almost identical in the range of q investigated here.

B. M-edge region of the encapsulated scandium atoms

Subsequent to the initial experimental report of a $Sc_3N@C_{80}^+$ single-photoionization cross-section contribution of the scandium atoms encapsulated inside a C_{80} sphere [21], Korol and Solov'yov published a prediction of narrow autoionization resonances in the excess cross section caused by the presence of the three Sc atoms in the endohedral fullerene [28]. The absence of these resonances in the first experiment [21] might have been attributed to the limited statistical quality and low density of the previous cross section measurements.

As part of this experimental effort, the cross section for single-photon single ionization of $Sc_3N@C_{80}^+$ ions was measured again with a step size of 20 meV compared to the previous 400 meV. The energy range 25 – 52.5 eV was covered. Statistical uncertainties near the maximum excess cross section of approximately 6% were accomplished compared to the previous 20%. The energy res-
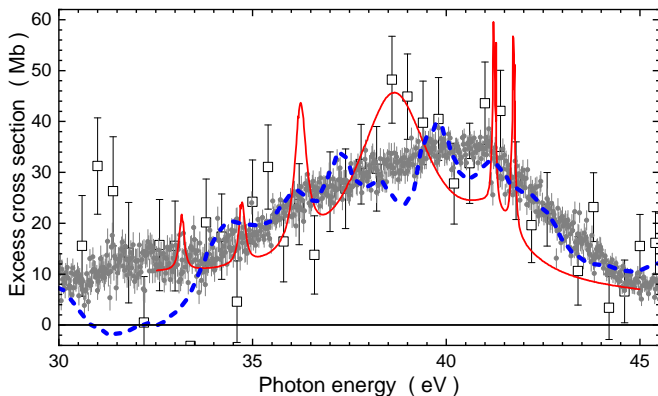
FIG. 6. (color online) Excess cross section originating from the encapsulated Sc_3N cluster relative to the C_{80} cage. Previous experimental results [21] are represented by open squares with statistical error bars. The present new data are the gray circles with smaller statistical uncertainties. The solid (red) line is the result published by Korol and Solov'yov [28] for a radial distance $r_{Sc} = 0.55 r_{cage} = 0.23$ nm of the Sc atoms from the center of the endohedral fullerene where $r_{cage} = 0.415$ nm is the average radius of the C_{80} shell used in their calculation. The (blue) dashed line is the result (for total photoabsorption) of Chen and Msezane [29] divided by 12.

olution was similar in both experiments: 85 meV in the new measurement and 100 meV in the previous experiment.

Figure 6 compares the new and the previous experimental results for single ionization of $Sc_3N@C_{80}^+$ ions by single photons in the energy range of interest with theoretical excess cross sections. The spectrum calculated by Korol and Solov'yov [28] shows clear signatures of scandium autoionization resonances while the structures in the cross section obtained by Chen and Msezane [29] are typical of fluctuations resulting from (time-dependent) DFT. The new experimental results show no evidence of resonances and other structural features predicted by the calculations.

In both theoretical treatments the dependence of the excess cross section for photoionization of $Sc_3N@C_{80}$ on the off-center position of the Sc atoms is emphasized. Small deviations of the radial distance r_{Sc} of the Sc atoms from the center of the whole endohedral molecule relative to the average radius r_{cage} of the cage can lead to significant broadening of autoionizing resonances. In particular, an increasing ratio r_{Sc}/r_{cage} causes the resonancees to be smeared out. A ratio $r_{Sc}/r_{cage} = 0.6$ approximately doubles the Lorentzian widths of the dominant scandium resonances. Thus, one of the possible explanations is that the theoretical ratio r_{Sc}/r_{cage} is too small. However, previous detailed investigations [51, 61] of the $Sc_3N@C_{80}$ geometry indicate values for $r_{Sc} = 0.20$ nm and $r_{cage} = 0.41$ nm which result in $r_{Sc}/r_{cage} = 0.49$, much smaller than the limit where resonances are predicted to disappear. Another effect not considered in the calculations is the temperature of the $Sc_3N@C_{80}$

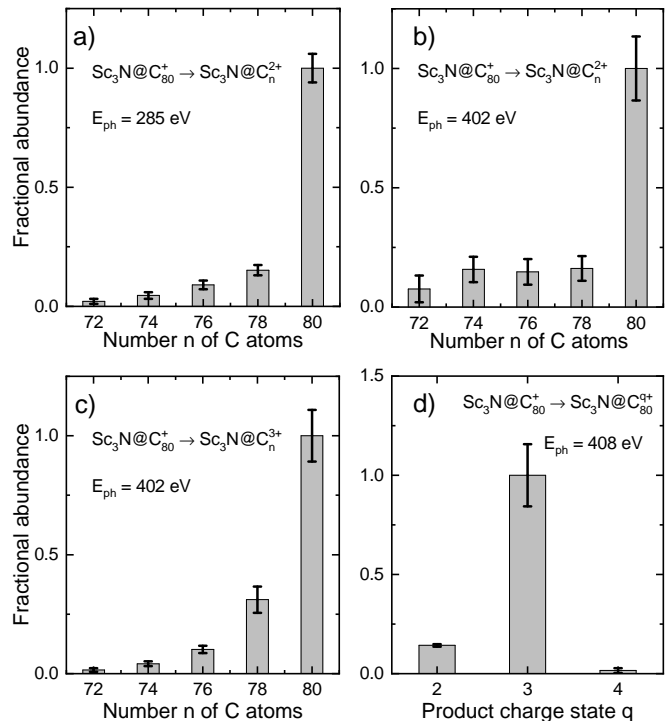
FIG. 7. Fractional abundances of different product ions measured after the absorption of a single photon by $Sc_3N@C_{80}^+$ ions; a) $Sc_3N@C_n^{2+}$ products at photon energy $E_{ph} = 285$ eV with $n = 72, 74, 76, 78, 80$; b) the same products at $E_{ph} = 402$ eV; c) $Sc_3N@C_n^{3+}$ products at photon energy $E_{ph} = 402$ eV with $n = 72, 74, 76, 78, 80$; d) $Sc_3N@C_{80}^{q+}$ products at photon energy $E_{ph} = 408$ eV with $q = 2, 3, 4$. Vertical bars indicate the experimental uncertainties of the measured abundances.

molecule. In the experiments the endohedral-fullerene powder has to be evaporated, which requires oven temperatures exceeding 600 K. The plasma environment in the ion source may lead to further heating which is not controllable in the experiment. With 249 internal degrees of freedom, the thermal energy stored in the $Sc_3N@C_{80}$ molecule is almost 13 eV already at 600 K. The associated kinetics are likely to broaden and thus smear out resonances arising from single Sc atoms.

C. Product-ion yields and cross sections

Absolute cross sections σ in merged-beams experiments are obtained from

$$\sigma = R \frac{q e v_{ion}}{\eta \phi_{ph} I_{ion} \mathcal{F}_L} \quad (1)$$

with the signal count rate R, the charge state q of the parent ions, the elementary charge e, the ion velocity v_{ion}, the signal-detection efficiency η, the photon flux ϕ_{ph}, the electrical current I_{ion} of the parent ions, and the form factor $\mathcal{F}_L$ [10]. In a given experiment with observation

of product channels for a specific parent ion species most quantities in Eq. 1 are constant. Experience with the PIPE setup used in the present experiments shows that the form factor does not significantly vary with photon energy in the investigated range. Thus the absolute cross sections obtained in an energy-scan measurement are proportional to the signal yield defined by

$$Y = \frac{R}{\phi_{\text{ph}} I_{\text{ion}}}. \tag{2}$$

With exception of the low-energy measurements covering contributions of Sc M-shell ionization, the present data are not absolute and product ion yield measurements were performed as functions of the photon energy. In order to put the yield curves on proper relative scales, separate measurements were conducted in which, at a fixed photon energy, the yields were measured for different reaction channels of one given parent ion under identical experimental conditions. Examples for such sets of yields are given in Fig. 7. In each data set the yield of the dominating final channel is normalized to 1. Clearly, in the measurements of processes $Sc_3N@C_{80}^+ \rightarrow Sc_3N@C_n^{2+} + e + (80 - n)/2 \times C_2$ with $n = 72, 74, 76, 78, 80$ (panels 7a and 7b) the ionization without fragmentation ($n = 80$) is by far the most important channel. Similarly, double ionization without fragmentation dominates over the channels involving double ionization with fragmentation (panel 7c). When comparing single, double and triple ionization without fragmentation of the initial $Sc_3N@C_{80}^+$ ion at $E_{\text{ph}} = 408$ eV (panel 7d) double ionization is by far the dominant channel.

Yield spectra, i.e., product-ion yields as a function of photon energy, were measured at a fixed monochromator-exit-slit width of 1500 μm resulting in a photon energy resolution at 400 eV of 1.1 eV. This was evidenced by the measurement of the vibrational levels in the N_2 $1s \rightarrow \pi*$ absorption spectrum. Spectra were obtained for $Sc_3N@C_{80}^+$ parent ions and the three dominant product channels $Sc_3N@C_{80}^{2+}$, $Sc_3N@C_{78}^{2+}$, and $Sc_3N@C_{80}^{3+}$. By using the fractional-abundance measurements shown in Fig. 7 the measured yield spectra for $Sc_3N@C_{80}^+$ parent ions were put on a relative scale. Moreover, the data of Fig. 7 suggest that about 70% of the total photoabsorption by $Sc_3N@C_{80}^+$ ions at photon energies slightly above 400 eV is accounted for by these three channels. The total photoabsorption cross section, in turn, can be inferred from the compilation provided by Henke et $al.$ [44]. Thus, approximate cross sections for the three dominant photoprocesses of $Sc_3N@C_{80}^+$ ions can be obtained. The results are shown in Fig. 8 panels a), b), and c) with their statistical error bars. The estimated total uncertainties are ±50%.

As described in Sect. II, the cross section for double detachment of $Sc_3N@C_{80}^-$ parent ions was obtained by assuming a typical form factor with an estimated uncertainty of a factor of 2. The measurement was also carried out with an energy resolution of 1.1 eV. The result
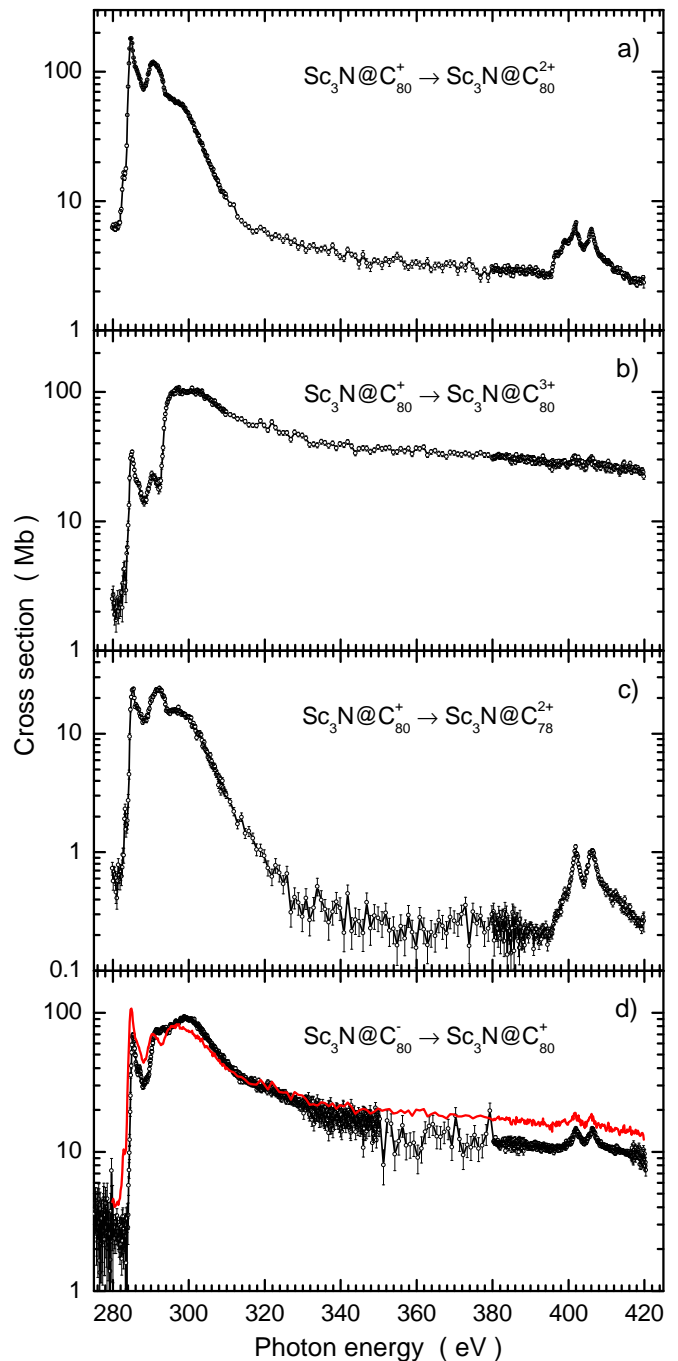

FIG. 8. (color online) Overview of the measured cross sections as functions of the photon energy. For normalization procedures and associated uncertainties see main text. The experimentally derived cross sections are shown as open circles with their statistical uncertainties. The investigated processes are indicated in each panel. The solid (red) line in panel d) is the average of single- and double-ionization cross sections for $Sc_3N@C_{80}^+$ parent ions.

is given by the data points with statistical uncertainties in panel d). Exploration of possible other final channels with different charge states and different levels of fragmentation demonstrated that double detachment is the strongest photoprocess accessible to the experiment (single detachment forming neutral $Sc_3N@C_n$ was not observable). The spectrum obtained for double detachment of $Sc_3N@C_{80}^-$ shows features occurring in both single and double ionization of $Sc_3N@C_{80}^+$. Therefore, it is meaningful to model the double-detachment cross section for the negative ion by a linear combination of the single- and double-ionization cross sections of the positive ion. The red curve in panel d) is the average of these latter two cross sections, i.e., identical weight factors of 0.5 were used for the two contributing spectra. The result is within 30% of the cross section for double detachment of $Sc_3N@C_{80}^-$.

All cross-section functions show a sharp rise with a resonance feature at about 285 eV and a number of resonances below the carbon K-shell ionization threshold at about 290 eV in $Sc_3N@C_{80}^-$ and about 294 eV in $Sc_3N@C_{80}^+$. At photon energies between 395 and 410 eV, additional cross-section contributions arising from the encapsulated Sc_3N cluster are visible. These contributions are investigated more closely in the following subsections.

The present results clearly show that the dominant photoprocesses of $Sc_3N@C_{80}^-$ and $Sc_3N@C_{80}^+$ ions are direct single and double ionization while fragmentation is of minor importance. This is in stark contrast to recent experiments by Xiong et al. [12] who investigated soft-x-ray-induced ionization and fragmentation dynamics of neutral $Sc_3N@C_{80}$ using an ion-ion-coincidence momentum-imaging technique. At a photon energy of 406.5 eV they found dominant channels leading to complete disintegration of the endohedral fullerene into small fragments. Single and multiple ionization without fragmentation were found to be less probable than the release of a single Sc^+ product ion. Almost no pure single ionization without fragmentation was observed and triple ionization without fragmentation was the dominant pure multiple-ionization channel in their experiment. In the present experiment, pure double detachment is the dominant process for $Sc_3N@C_{80}^-$ and pure single and double ionization are dominant for $Sc_3N@C_{80}^+$ ions.

At 406.5 eV, absorption of the incoming photon by one of the Sc atoms is an important contribution to the total photoabsorption cross section. At this energy, excitation of the L_2 subshell of Sc is the most likely process. Previous experiments on photoionization of neutral Sc atoms [57] showed that triple and double ionization are the dominant final channels resulting from L-shell excitation of neutral Sc. However, the Sc atoms encapsulated inside a C_{80} sphere are known to have an average electrical charge of +2.3 [26], i.e., each Sc atom donates a charge equivalent to 2.3 electrons to the C_{80} sphere and the central N atom. Hence, it is more appropriate to consider the final decay channels of Sc^{2+} and Sc^{3+} after L-shell excitation. Experimental data are not available

for these charge states but a theory-based analysis has been carried out by Kaastra and Mewe [62] who find predominantly single or double ionization as the result of the decay of a $2p$ vacancy in Sc^{2+} and single ionization as the result of the decay of a $2p$ vacancy in Sc^{3+}. For neutral carbon they find predominantly single Auger decay after the production of a K-shell vacancy. Previous measurements with $Xe@C_{60}^+$ [24] showed that the charge state distribution of the endohedral molecule after photoionization of the $4d$ subshell of the encapsulated xenon atom was similar to that of free (neutral) xenon after $4d$ photoionization. The present experiment follows this same scheme with encapsulated and free $Sc^{2+/3+}$, given the results of Kaastra and Mewe.

From the present experiment and the analysis provided in the previous paragraph one may conclude that high stages of ionization and predominant cage destruction observed in the experiment by Xiong et al. [12] have to be attributed to the special conditions in their experiment. Two possible explanations for their observation come to mind. One is the high oven temperature of about 910 K which might have resulted in partial thermal and subsequently also chemical decomposition of the heated sample. Moreover, at such a high temperature $Sc_3N@C_{80}$ is evaporated with a large amount of vibrational energy substantially exceeding the lowest ionization and fragmentation thresholds. The second is the detection probability of the ion detector in their time-of-flight spectrometer. At the acceleration voltage used for the product ions, a strong variation of the detector efficiency is to be expected for fragments with different charge states and energies. This was not considered in the paper by Xiong et al. One should also keep in mind that 97% purity of the original sample, as used in their experiments, does not guarantee the identical purity of the vapor produced at a given temperature from that sample due to the effect of fractional evaporation of sample components that have very different vapor pressures. It should be mentioned in this context that the main body of results obtained by Xiong et al. is based on momentum-resolved multi-coincidence spectra which are not influenced by several of the caveats discussed above.

D. Scandium L-edge and nitrogen K-edge region of the encapsulated Sc_3N metal nitride cluster

The main focus of the present work is on the cross-section features caused by the encapsulated Sc_3N cluster. The double-peak structure observed near 400 eV is caused by L-shell excitation of the scandium atoms and K-shell excitation of the nitrogen atom. Figure 9 zooms into the associated energy regions of the spectra provided by Fig. 8. In addition to the magnifications shown in panels 9a, 9b, 9c, and 9e the corresponding energy range in the previously reported absorption spectrum of neutral crystalline $Sc_3N@C_{80}$ [27] is included (panel 9d).
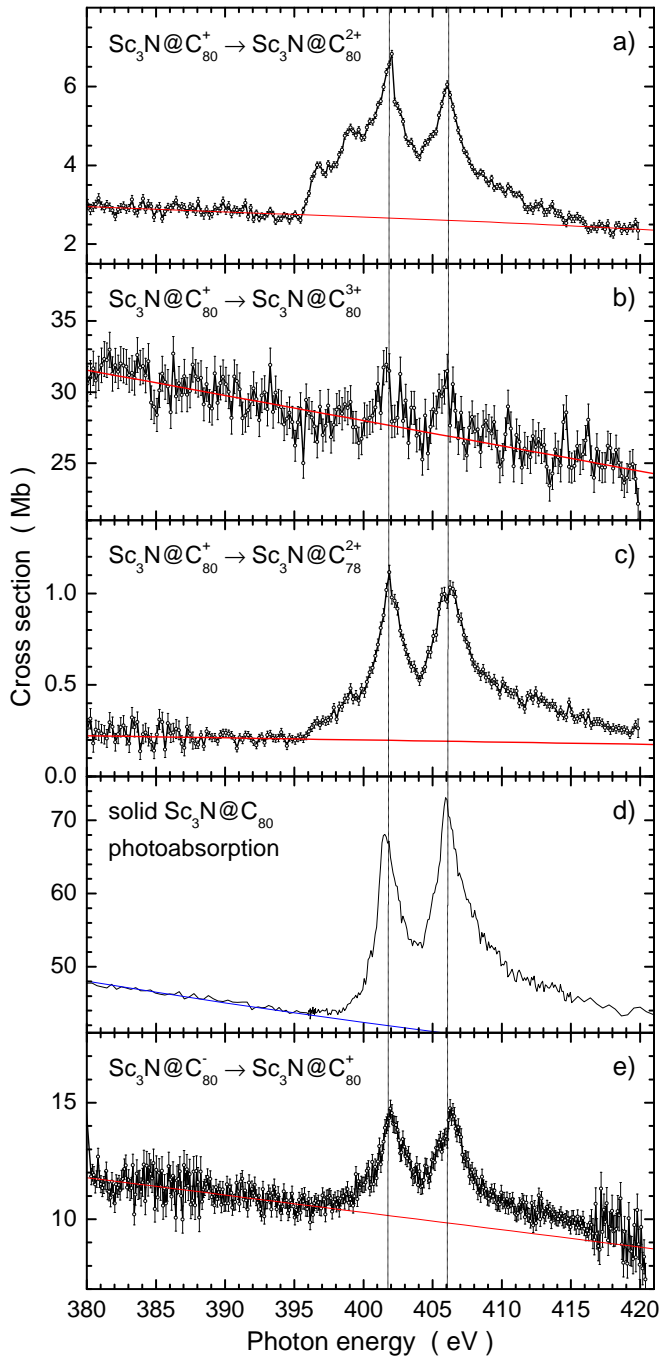
The resonance features of interest are all similar but

FIG. 9. (color online) Cross sections of photoprocesses involving positive $Sc_3N@C_{80}^+$ ions (panels a, b, and c), neutral crystallized $Sc_3N@C_{80}$ (panel d) and negative $Sc_3N@C_{80}^-$ ions (panel e) in the photon energy range of the K edge of nitrogen and the L edge of scandium. Panels a, b, c, and e provide details of the spectra shown in Fig. 8. Panel d is a detail of the absorption spectrum obtained previously by Müller *et al.* [27]. The specific channels are identified in the figure along with each spectrum. Vertical dashed lines mark the peak energies of the dominating Sc resonance features. The solid (red and blue) lines in each panel are extrapolated cross sections representing the "background" cross-section contribution of the C_{80} shell.
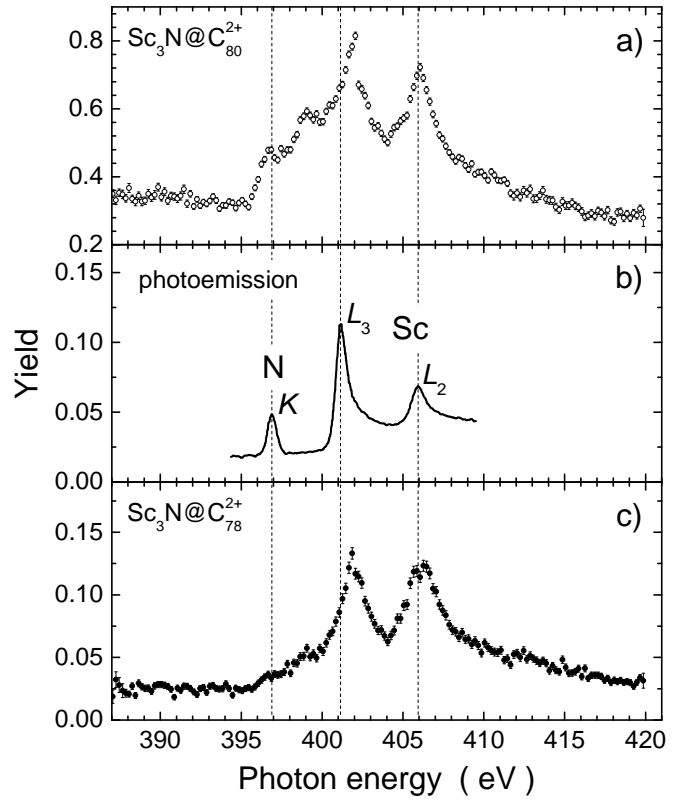

FIG. 10. Contributions of the Sc_3N cluster to the yields obtained for various photoprocesses involving $Sc_3N@C_{80}^+$ (panels a and c) and neutral $Sc_3N@C_{80}$ (panel b, adapted from previous work by Alvarez *et al.* [26]). The data in panels a and c correspond to the ones shown in Fig. 9, panels a and c, respectively. Panel b shows the core-level photoemission spectrum of the Sc $2p$ and N $1s$ lines in the neutral endohedral fullerene measured as a function of photon energy. The peak assignments provided by Alvarez *et al.* are indicated in panel b. The vertical dashed lines mark the positions of the resonances seen in panel b.

not identical. They are superimposed on a "background" arising from photoionization of the C_{80} sphere. Depending on the individual channel, the "background" levels and resonance peak heights are very different. For double ionization of $Sc_3N@C_{80}^+$ (panel b) the fingerprint of the Sc_3N cluster is very weak compared to the contribution of the C_{80} cage. As a result the statistical quality of the peak features is not as good as in the measurements for the other channels investigated.

The main peaks in the spectra shown in Fig. 9 line up in energy quite well although the parent target charge state varies from +1 to -1 and different exit channels are observed. Lining up of peak energies for different charge states is also found in the present model calculations (see Fig. 5. However, notwithstanding the similarity in peak positions, the individual spectra shown in Fig. 9 significantly differ from one another. In particular, the single-ionization spectrum shows structural features that are strongly suppressed in all other spectra. For further dis-

cussion of differences it is worthwhile investigating which processes contribute to the spectral features. The required information is obtained from the measured yield of photoemission from core-level photoexcited $Sc_3N@C_{80}$ previously obtained by Alvarez *et al.* [26] together with their assignment of the peak features shown in panel b of Fig. 10.

In addition to the photoemission yield spectrum measured by Alvarez *et al.* [26] for neutral $Sc_3N@C_{80}$, Fig. 10 also includes the yields obtained in the present experiments for the photoprocesses $Sc_3N@C_{80}^+ \rightarrow Sc_3N@C_{80}^{2+}$ (panel a) and $Sc_3N@C_{80}^+ \rightarrow Sc_3N@C_{78}^{2+} + C_2$ (panel c). The two spectra are remarkably different near the low-energy side of the Sc L_3 feature where single ionization shows much more strength than single ionization accompanied by emission of a neutral C_2 dimer. By comparison with the results provided in panel b one may conclude that the rapid increase in the measured single-ionization spectrum at 396 eV (see panel a) is due to K-shell excitation of the encapsulated nitrogen atom.

According to Kaastra and Mewe [62], a K vacancy in nitrogen predominantly decays by a single Auger process, i.e., a K-shell photoexcitation resonance in nitrogen primarily leads to a resonance in the single-ionization of the nitrogen atom. The fact that the nitrogen atom is encapsulated by the C_{80} cage has apparently little influence on the final result of the initial N1s photoexcitation: The whole endohedral fullerene ion just changes its charge state by one unit. Very little effect of the presence of the N atom is seen in the $Sc_3N@C_{78}^{2+} + C_2$ product channel. One may conclude that the Auger electron emitted from the nitrogen atom which is known to be near the center of the C_{80} cage has little interaction with the valence electrons of the carbon cage.

On the other hand, there is a relatively sizable effect of photoabsorption by the three Sc atoms on the formation of $Sc_3N@C_{78}^{2+}$ although the emitted Auger electron has roughly the same energy as that emitted by the N atom. A possible explanation for this difference is the position of the three Sc atoms close to the inner surface of the C_{80} cage with some bonding to three of the carbon pentagons [63] that constitute the C_{80} structure together with carbon hexagons. When one of the Sc atoms undergoes an Auger decay subsequent to L-shell excitation the valence shell is disturbed and, with it, also the bonding to the inner surface of the carbon cage. Another possible mechanism for efficient charge transfer from the carbon cage to the inner-shell excited Sc atom could be interatomic Coulombic decay (ICD) [64, 65], i.e., a two-center Auger process, where a carbon K-shell or L-shell electron fills the Sc 2p vacancy and an outer shell electron either from the carbon atom or the scandium atom is emitted. As a result of charge transfer from the carbon cage to the photoionized Sc atom, fragmentation of the intermediate $Sc_3N@C_{80}^{2+}$ ion is a likely process that overwhelms possible contributions from the decay of a K vacancy in the central N atom.

The dominant resonance features in photoabsorption
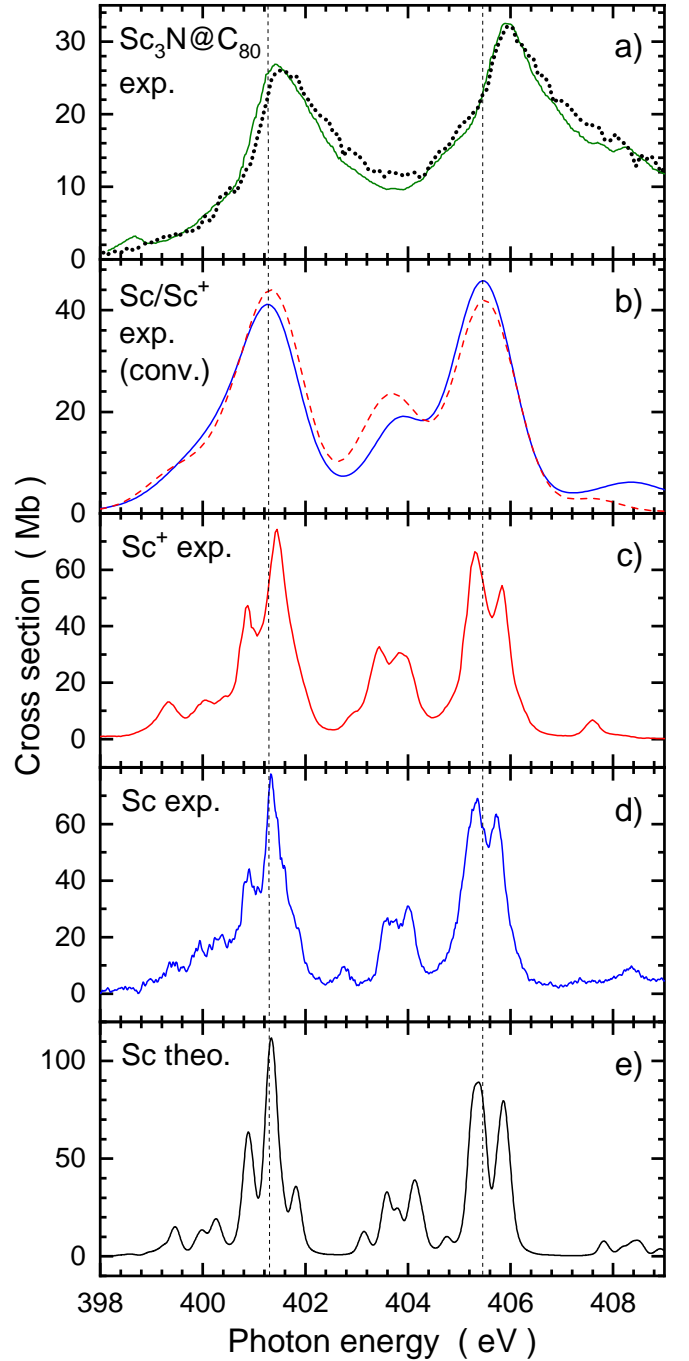

FIG. 11. (color online) Comparison of photoabsorption cross sections (all adapted from previously published work) of Sc_3N in neutral $Sc_3N@C_{80}$ (panel a) with experimental and theoretical results for neutral Sc and singly charged Sc^+ ions (panels b,c,d,e). Panel a: Photoabsorption by Sc_3N in crystalline $Sc_3N@C_{80}$ [27] with the contribution of C_{80} subtracted (dotted line); photoabsorption by Sc_3N in $Sc_3N@C_{80}$ sublimated on a clean single crystalline Au(110) surface [26] with the contribution of C_{80} subtracted (solid line). Panel b: Photoabsorption by neutral Sc atoms [57] (solid line) and photoabsorption by Sc^+ ions [58] (dashed red line); measured yields were normalized to theory for neutral Sc and convoluted with a 1-eV FWHM Gaussian distribution function. Panel c: Photoabsorption by Sc^+ ions [58] normalized to theory for neutral Sc. Panel d: absorption by neutral Sc atoms [57] normalized to theory. Panel e: theoretical absorption cross section for neutral Sc atoms [57, 66].

by neutral $Sc_3N@C_{80}$ are due to the encapsulated scandium atoms. Therefore, it is useful to compare these features with those found by theory and experiment for neutral Sc and for Sc^+ ions. Panel a of Fig. 11 shows normalized cross sections (see above) for neutral $Sc_3N@C_{80}$ deposited on metal surfaces. The dotted line is the result published by Müller *et al.* [27], the solid line represents a measurement by Alvarez *et al.* [26]. The two spectra obtained in different experiments are almost identical in shape. The contributions of both the scandium L shell and the nitrogen K shell are evident in these total-absorption data.

For comparison, Fig. 11 includes experimental photoabsorption spectra of neutral Sc [57] (panel d) and singly charged Sc^+ ions [58] (panel c), both in the gas phase. The measurements on neutral Sc were accompanied by a calculation of the photoabsorption cross section [57, 66]. The theoretical photoabsorption spectrum (panel e) was convoluted with a 0.1-eV full-width-at-half-maximum (FWHM) Gaussian to simulate the experimental photon-energy bandwidth and is in reasonable agreement with the experiment.

While the photoabsorption spectra of Sc and Sc^+ show numerous fine details that are related to individual transitions to specific excited states, the absorption by neutral $Sc_3N@C_{80}$ is a much smoother function of photon energy. The reason for this is not the limitation in experimental resolution but the effect of hybridization of the valence shells of the encapsulated atoms and the surrounding carbon shell. For better comparison, the experimental spectra of free Sc and Sc^+ were convoluted with a 1-eV FWHM Gaussian distribution function to simulate the hybridization effect. The results are shown in panel b. The solid (blue) line is obtained from the experiment with neutral Sc, the dashed (red) line from the experiment with Sc^+ ions. The two contributions associated with excitations of the L_3 and L_2 subshells peak at almost identical energies indicated by the vertical dashed lines. The same Sc features found in the endohedral fullerene occur at slightly higher energies as evidenced by the extension of the vertical lines into panel a. The shifts of the observed peaks are of the order of 1 to 1.5 eV.

In addition to the resonance positions and the shapes of the measured spectral contributions of the encapsulated Sc_3N cluster, the sizes of the related partial cross sections are of interest. For comparison of the experimental data, the "background" originating from the C_{80} cage has been subtracted from the cross sections displayed in Fig. 9. This "background" cross section may be reasonably approximated by straight lines in the energy range of interest, as indicated in Fig. 9. The isolated partial Sc_3N cross-section contributions obtained from the present measurements after "background" subtraction are displayed in Fig. 12. Again, the vertical lines indicate the positions of the two main peak features. The statistical quality of the data for single ionization (panel a) is quite different from that for double ionization (panel
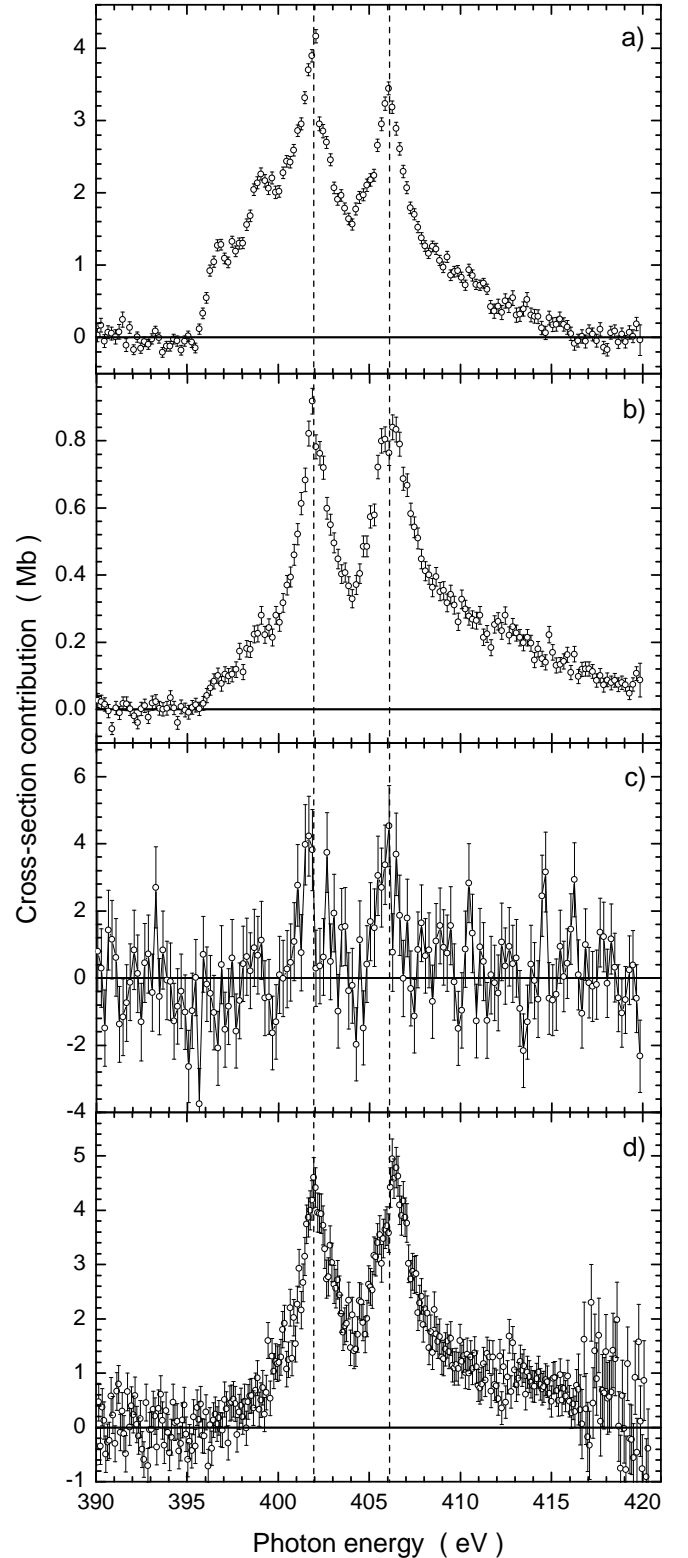

FIG. 12. The isolated contributions of the Sc_3N cluster within $Sc_3N@C_{80}^+$ (panels a, b, and c) and within $Sc_3N@C_{80}^-$ (panel d), respectively, to the cross sections for the formation of $Sc_3N@C_{80}^{2+}$ (panel a), of $Sc_3N@C_{78}^{2+}$ (panel b), of $Sc_3N@C_{80}^{3+}$ (panel c), and of $Sc_3N@C_{80}^+$ (panel d).

c) although the overall size of the cross sections is very similar. The reason for this is the strong contribution of carbon K-shell ionization of the C_{80} cage and subsequent single-Auger decay. Much better contrast between the Sc_3N signal and the C_{80} "background" is obtained for the single-ionization plus fragmentation channel (panel b) although the cross section for the encapsulated cluster is smaller by a factor of approximately 5.

The size of the contribution of Sc_3N to double-detachment of $Sc_3N@C_{80}^-$ is approximately equal to the contribution of Sc_3N to double-ionization of $Sc_3N@C_{80}^+$. Because of a smaller "background" cross section of the C_{80} cage the statistical quality of the negative-ion double-detachment data is much better than that of the positive-ion double-ionization measurement.

A surprise in this investigation was the observation of Sc $3d$ excitation features in $Sc_3N@C_{80}^+$ and $Sc_3N@C_{80}^-$ at identical photon energies. The two different initial charge states of the endohedral fullerene had been chosen to produce a maximum change of the electrical charge distribution inside the cage and to search for differences in the photoabsorption cross section (including an energy shift). That the observed $3d_{5/2}$ and $3d_{3/2}$ excitation features line up with one another indicates that the resonance energies of the encapsulated atoms are little influenced by the initial charge of the endofullerene.

The question of actual charges ζ on the atoms constituting $Sc_3N@C_{80}^q$ has been addressed in our model calculations. Previously, Alvarez *et al.* [26] found that the carbon cage with $q = 0$ carries the charge $\zeta(C_{80})$=-6.3e, i.e., each scandium atom gives up 2.4e and the nitrogen atom absorbs 0.9e. The present model calculations carried out at the level described in Sec. III suggest lower charges on the atoms of $Sc_3N@C_{80}$. The computations yielded $\zeta(Sc)$=+1.2e, $\zeta(N)$=-1.2e, and $\zeta(C_{80})$=-2.3e in the Mulliken approach [59] and $\zeta(Sc)$=+0.6e, $\zeta(N)$=-0.5e, and $\zeta(C_{80})$=-1.4e from the Löwdin [60] analysis. In their 2013 review on endohedral fullerenes Popov, Yang and Dunsch [5] state that for the Sc_3N cluster "The charges strongly depend both on the method of theory used to compute wave functions and on the electron density partitioning, but all reported values are significantly smaller than +6 expected for the purely ionic $(Sc_3N)^{6+}@C_{80}^{6-}$."

In spite of the differences between computations of the actual charge on the constituents of the trimetallic nitride cluster fullerene, the present Mulliken- and Löwdin-charge calculations agree on the development along the sequence of $Sc_3N@C_{80}^q$ molecules in charge states $q = -1, 0, +1, ..., +4$ demonstrating that the charges of the encapsulated nitrogen and scandium atoms remain essentially unchanged while the charge state q of the endofullerene is varied by up to six units. The relatively small influence of the overall charge state of the endohedral fullerene on the charge of the encapsulated Sc atoms is confirmed for $q = 0$ and $q = -1$ by a previous investigation authored by Popov and Dunsch [67]. Transferring this finding to the charge on the carbon cage in the neutral fullerene as derived by Alvarez *et al.* means that for $q = -1$ the cage carries a charge of $-7.3e$ and for $q = +4$ the charge on the cage is reduced to -2.3 e. At the same time each Sc atom and the nitrogen atom essentially maintain their charge $\zeta(Sc)$=+2.4e and $\zeta(N)$=-0.9e. As a result, the cross section for photoabsorption by the encapsulated Sc_3N nitride cluster is not expected to change with q. Indeed, the present DFT calculations confirm this expectation as demonstrated by Fig. 5.

E.   Carbon K-edge region

The measured product-ion yields (and hence also the inferred cross sections) show pronounced resonance and threshold features near the K edge of carbon. Fig. 13 zooms into the lower-energy region of the spectra displayed in Fig. 8 to emphasize the carbon K-edge region. Similar to the results obtained previously with $Lu_3N@C_{80}$ ions in different charge states [15], the cross sections all show contributions of certain base features. The vertical lines in Fig. 13 demonstrate that resonances as well as signatures of the K-shell photoionization threshold line up with one another in the different final product channels. The dashed line at 284.8 eV is approximately at the position of the first narrow resonance occurring in all of the spectra. The solid line at 290.2 eV marks what is considered to be the K-shell ionization threshold of a carbon atom in the $Sc_3N@C_{80}^-$ ion. The solid line at 293.8 eV is meant to mark the K-shell ionization threshold of a carbon atom in the $Sc_3N@C_{80}^+$ ion. A carbon K-shell vacancy predominantly decays by a single-Auger process so that net double ionization of a carbon atom results when the K shell is ionized. When transferring this finding to the fullerene, a double-ionization onset at the K edge is expected. This is the basis of the assignments of the two lines discussed above. The exact positions of the K-shell ionization threshold energies inferred from the threshold steps in Fig. 13 have uncertainties due to the absolute calibration of the photon-energy scale and due to the width of the edge features. The 3.6-eV difference of the two energies has an estimated uncertainty of 0.6 eV.

The difference of $\Delta E = (3.6 \pm 0.6)$ eV between the thresholds for carbon K-shell ionization in $Sc_3N@C_{80}^-$ and in $Sc_3N@C_{80}^+$ might be used to extract information about the outer radius of the endohedral molecule similar to the analysis published previously [15]. The simplest approach is to assume that the difference is given by

$$\Delta E = \frac{1}{4\pi\epsilon_0} \frac{e\delta q}{R}, \tag{3}$$

where R is the outer radius of the fullerene sphere and δq the charge difference between the negatively and positively charged fullerene. The quantities e and ϵ_0 are the elementary charge and the electrical constant. Assuming $\delta q = 2e$ one obtains a value of R of 0.8 nm which is much higher than the radius found previously.
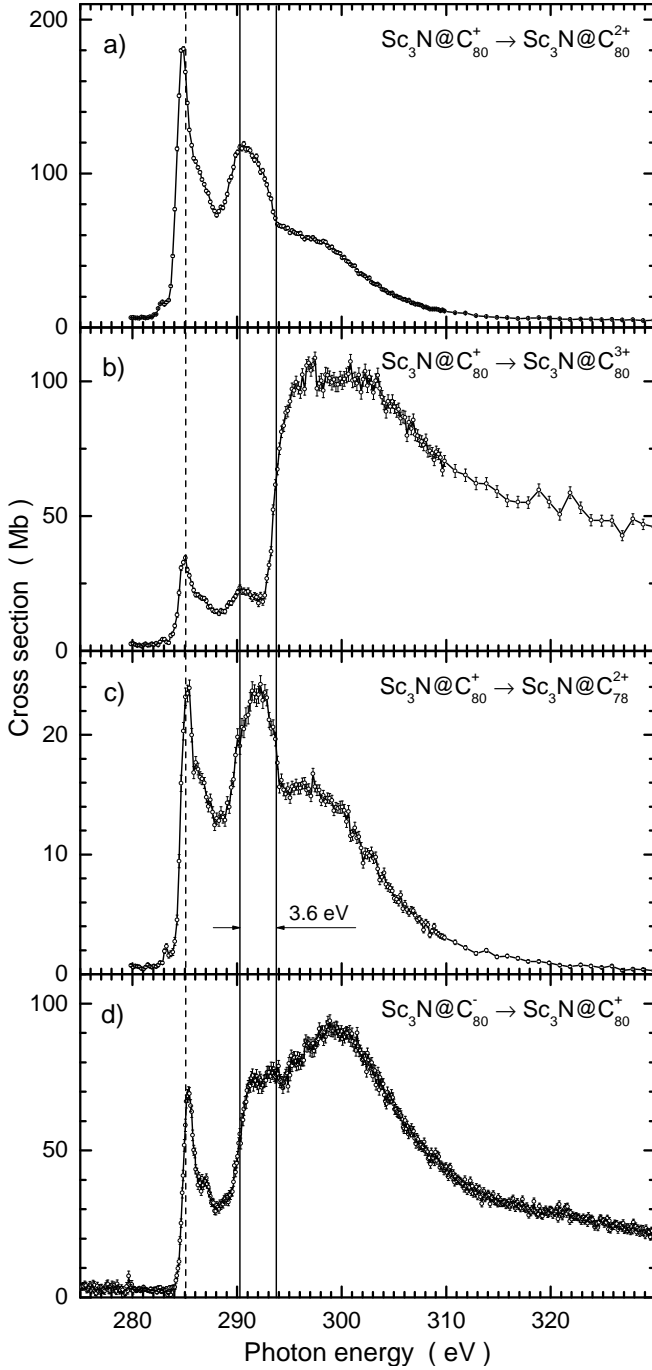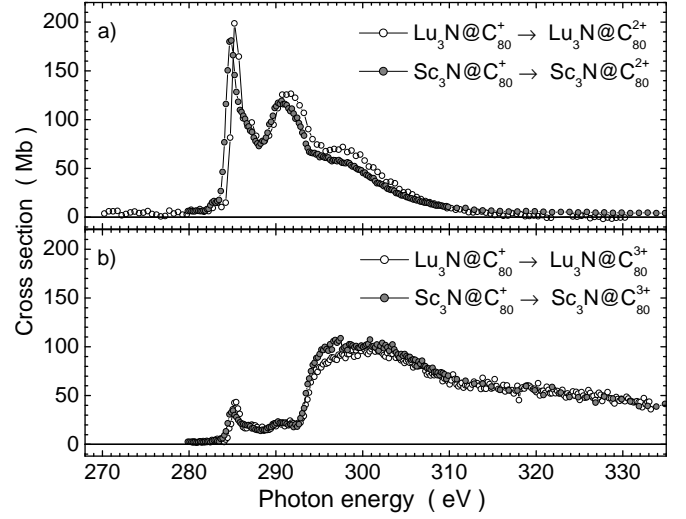
FIG. 14. Comparison of the present spectra for $Sc_3N@C_{80}^+$ (solid data points) near the carbon K edge with previously published measurements for $Lu_3N@C_{80}^+$ [15] (open circles) for single ionization (panel a) and double ionization (panel b).

While one may assume that the positive charge on the $Sc_3N@C_{80}^+$ sphere is uniformly distributed over the surface, the attached electron in the $Sc_3N@C_{80}^-$ ion is freely movable around the sphere and will move away from other negative charges. When the K-shell photo-electron leaves the sphere, the attached electron is likely to move to the opposite side of the cage. Hence, the electron has to overcome the potential energy associated with $2R$. Accordingly, the difference ΔE is now

$$\Delta E = \frac{e^2}{4\pi\epsilon_0}\left[\frac{2}{R} - \left(\frac{1}{R} - \frac{1}{2R}\right)\right] \qquad (4)$$

which yields $R = 0.6 \pm 0.1$ nm. Considering the uncertainty of ΔE this is in agreement with the previous finding of 0.5 ± 0.04 nm [15]. It is also in agreement with the van-der-Waals radius of C_{80} with I_h symmetry that has been found to be between 0.53 and 0.56 nm by using quantum molecular dynamics calculations [68]. The present radius R can also be associated with the radius r_{cage} discussed in Sect. IV B. When adding the half-thickness of the carbon cage to the average radius r_{cage} of the cage one should get R. For the thickness of the C_{60} cage a value of 0.15 nm has been experimentally determined [69]. With $r_{cage} = 0.41$ nm for the C_{80} cage the outer radius of the fullerene sphere $R = 0.49$ nm results, which is still in accord with the present finding given the uncertainty of the C_{80} cage thickness.

In the case of $Lu_3N@C_{80}$ ions an analysis was carried out to determine which peak or threshold feature contributes to the individual final product ion channel with what amplitude [15]. Rather than repeating such an analysis here, we compare cross sections for photoprocesses of $Sc_3N@C_{80}^+$ with the related process of $Lu_3N@C_{80}^+$. Two of all the available spectra can be considered because they were measured for equivalent product channels of

FIG. 13. Cross sections of photoprocesses involving positive $Sc_3N@C_{80}^+$ ions (panels a, b, and c) and negative $Sc_3N@C_{80}^-$ ions (panel d) in the photon energy range of the K edge of carbon. The panels provide details of the overview spectra shown in Fig. 8. The specific channels are identified in the figure along with each spectrum. Vertical dashed and solid lines indicate the energies of characteristic cross-section features (see main text). Note the linear scale as compared to the logarithmic scale of Fig. 8.

both endohedral fullerenes. The results are shown in Fig. 14 where the yields obtained in the single- and double-ionization experiments with $Lu_3N@C_{80}^+$ are normalized by one constant factor to the related cross sections of $Sc_3N@C_{80}^+$ obtained in the present investigation. Small deviations in the positions of resonance features of $Sc_3N@C_{80}^+$ and $Lu_3N@C_{80}^+$ are attributed to the uncertainties of the associated energy calibrations.

V. SUMMARY AND OUTLOOK

Photoprocesses of the endohedral metallofullerenes $Sc_3N@C_{80}^+$ and $Sc_3N@C_{80}^-$ in the gas phase have been studied by experiments and by supporting model calculations.

Previous measurements on photoionization of $Sc_3N@C_{80}^+$ in the energy range 30 - 50 eV were repeated with much finer energy steps and improved statistical precision. The results rule out the theoretically predicted presence of narrow autoionizing Sc resonances in the photoionization cross section.

For $Sc_3N@C_{80}^+$ the product channels resulting in $Sc_3N@C_{80}^{2+}$, $Sc_3N@C_{80}^{3+}$, and $Sc_3N@C_{78}^{2+}$ were investigated in the photon energy range 280 to 420 eV. In the same range the double-detachment product channel $Sc_3N@C_{80}^+$ resulting from photoabsorption by the anion $Sc_3N@C_{80}^-$ was studied. The dominant processes are the removal of one or two electrons from the parent endohedral metallofullerene.

The observed relative magnitudes of product-ion yields may be understood in terms of the known Auger-decay probabilities of isolated atoms. All the final-channel spectra show distinct contributions from the encapsulated Sc_3N cluster as well as characteristic resonance features near the K edge of C. It is interesting to note that all cross-section features that are characteristic for the encapsulated cluster line up in energy, indicating that the charge on the encapsulated atoms does not significantly change when the charge state of the parent endofullerene is varied. This is in accord with the present model calculations.

The central N atom shows a distinct fingerprint on the single-ionization cross section of $Sc_3N@C_{80}^+$. Its importance relative to that of the Sc atoms appears to be enhanced in the single-ionization channel; however, the influence of the N atom is reduced in the single-ionization channel that includes fragmentation. The difference is explained by the central position of the N atom and its relatively large distance from the inner surface of the carbon cage in contrast to the small distance of the Sc atoms with their loose bonding to carbon pentagons which, together with carbon hexagons, establish the outer fullerene shell.

Finally, it was found that the cross-section functions for single and double ionization of $Sc_3N@C_{80}^+$ are almost identical with those for single and double ionization of $Lu_3N@C_{80}^+$, demonstrating the great similarity of the trimetallic nitride cluster fullerenes.

Experiments with internally cold endohedral fullerenes such as $Sc_3N@C_{80}^+$ would be highly desirable to eliminate effects of the substantial thermal energy that can be stored in the vibrational degrees of freedom. Measurements using radiofrequency ion traps or cryogenic storage rings are expected to provide better-defined initial conditions. Exposing trapped mass-selected endofullerenes to photon beams and analyzing the complete inventory of the trap after a given interaction time promises to provide access to all important final product channels simultaneously. Work in that direction is in progress.

VI. ACKNOWLEDGEMENTS

[1] H. W. Kroto, J. R. Heath, S. C. O'Brien, R. F. Curl, and R. E. Smalley, Nature **318**, 162 (1985).

[2] J. R. Heath, S. C. O'Brien, Q. Zhang, Y. Liu, R. F. Curl, F. K. Tittel, and R. E. Smalley, J. Am. Chem. Soc. **107**, 7779 (1985).

[3] Y. Chai, T. Guo, C. Jin, R. E. Haufler, L. P. F. Chibante, J. Fure, L. Wang, J. M. Alford, and R. E. Smalley, J. Phys. Chem. **95**, 7564 (1991).

[4] X. Lu, L. Feng, T. Akasaka, and S. Nagase, Chem. Soc. Rev. **41**, 7723 (2012).

[5] A. A. Popov, S. Yang, and L. Dunsch, Chem. Rev. **113**, 5989 (2013).

[6] A. A. Popov, ed., *Endohedral Fullerenes: Electron Transfer and Spin* (Springer International Publishing, 2017).

[7] I. Hertel, T. Laarmann, and C. Schulz, Adv. At. Mol. Phys. **50**, 219 (2005).

[8] V. K. Dolmatov, "Photoionization of atoms encaged in spherical fullerenes," in *Theory of Confined Quantum Systems: Part Two*, Advances in Quantum Theory, Vol. 58, edited by J. R. Sabin and E. Brändas (Academic Press, 2009) pp. 13 – 68.

[9] F. Lépine, J. Phys. B: At. Mol. Opt. Phys. **48**, 122002 (2015).

[10] S. Schippers, A. L. D. Kilcoyne, R. A. Phaneuf, and A. Müller, Contemp. Phys. **57**, 215 (2016).

[11] H. Xiong, L. Fang, T. Osipov, N. G. Kling, T. J. A. Wolf, E. Sistrunk, R. Obaid, M. Gühr, and N. Berrah, Phys. Rev. A **97**, 023419 (2018).

[12] H. Xiong, R. Obaid, L. Fang, C. Bomme, N. G. Kling, U. Ablikim, V. Petrovic, C. E. Liekhus-Schmaltz, H. Li, R. C. Bilodeau, T. Wolf, T. Osipov, D. Rolles, and N. Berrah, Phys. Rev. A **96**, 033408 (2017).

[13] C. M. Thomas, K. K. Baral, N. B. Aryal, M. Habibi, D. A. Esteves-Macaluso, A. L. D. Kilcoyne, A. Aguilar, A. S. Schlachter, S. Schippers, A. Müller, and R. A. Phaneuf, Phys. Rev. A **95**, 053412 (2017).

[14] K. K. Baral, N. B. Aryal, D. A. Esteves-Macaluso, C. M. Thomas, J. Hellhund, R. Lomsadze, A. L. D. Kilcoyne, A. Müller, S. Schippers, and R. A. Phaneuf, **93**, 033401 (2016).

[15] J. Hellhund, A. Borovik Jr., K. Holste, S. Klumpp, M. Martins, S. Ricz, S. Schippers, and A. Müller, Phys. Rev. A **92**, 013413 (2015).

[16] A. R. Milosavljević, A. Giuliani, and C. Nicolas, "Gasphase near-edge x-ray absorption fine structure (NEXAFS) spectroscopy of nanoparticles, biopolymers, and ionic species," in *X-ray and Neutron Techniques for Nanomaterials Characterization*, edited by C. S. S. R. Kumar (Springer, Berlin Heidelberg, 2016).

[17] J. Choi, E. H. Chang, D. M. Anstine, M. El-Amine Madjet, and H. S. Chakraborty, Phys. Rev. A **95**, 023404 (2017).

[18] S. W. J. Scully, E. D. Emmons, M. F. Gharaibeh, R. A. Phaneuf, A. L. D. Kilcoyne, A. S. Schlachter, S. Schippers, A. Müller, H. S. Chakraborty, M. E. Madjet, and J. M. Rost, Phys. Rev. Lett. **94**, 065503 (2005).

[19] S. W. J. Scully, E. D. Emmons, M. F. Gharaibeh, R. A. Phaneuf, A. L. D. Kilcoyne, A. S. Schlachter, S. Schippers, A. Müller, H. S. Chakraborty, M. E. Madjet, and J. M. Rost, Phys. Rev. Lett. **98**, 179602 (2007).

[20] R. C. Bilodeau, N. D. Gibson, C. W. Walter, D. A. Esteves-Macaluso, S. Schippers, A. Müller, R. A. Phaneuf, A. Aguilar, M. Hoener, J. M. Rost, and N. Berrah, Phys. Rev. Lett. **111**, 043003 (2013).

[21] A. Müller, S. Schippers, R. A. Phaneuf, M. Habibi, D. Esteves, J. C. Wang, A. L. D. Kilcoyne, A. Aguilar, S. Yang, and L. Dunsch, J. Phys. Conf. Ser. **88**, 012038 (2007).

[22] A. Müller, S. Schippers, M. Habibi, D. Esteves, J. C. Wang, R. A. Phaneuf, A. L. D. Kilcoyne, A. Aguilar, and L. Dunsch, Phys. Rev. Lett. **101**, 133001 (2008).

[23] A. L. D. Kilcoyne, A. Aguilar, A. Müller, S. Schippers, C. Cisneros, G. Alna'Washi, N. B. Aryal, K. K. Baral, D. A. Esteves, C. M. Thomas, and R. A. Phaneuf, Phys. Rev. Lett. **105**, 213001 (2010).

[24] R. A. Phaneuf, A. L. D. Kilcoyne, N. B. Aryal, K. K. Baral, D. A. Esteves-Macaluso, C. M. Thomas, J. Hellhund, R. Lomsadze, T. W. Gorczyca, C. P. Ballance, S. T. Manson, M. F. Hasoglu, S. Schippers, and A. Müller, Phys. Rev. A **88**, 053402 (2013).

[25] S. Stevenson, G. Rice, T. Glass, K. Harich, F. Cromer, M. R. Jordan, J. Craft, E. Hadju, R. Bible, M. M. Olmstead, K. Maitra, A. J. Fisher, A. L. Balch, and H. C. Dorn, Nature **401**, 55 (1999).

[26] L. Alvarez, T. Pichler, P. Georgi, T. Schwieger, H. Peisert, L. Dunsch, Z. Hu, M. Knupfer, J. Fink, P. Bressler, M. Mast, and M. S. Golden, Phys. Rev. B **66**, 035107 (2002).

[27] A. Müller, S. Schippers, R. A. Phaneuf, S. Scully, E. D. Emmons, M. F. Gharaibeh, M. Habibi, A. L. D. Kilcoyne, A. Aguilar, A. S. Schlachter, L. Dunsch, S. Yang, H. S. Chakraborty, M. E. Madjet, and J. M. Rost, in *Latest Advances in Atomic Cluster Collisions: Structure and Dynamics from the Nuclear to the Biological Scale*, edited by J.-P. Connerade and A. V. Solov'yov (Imperial College Press, London, UK, 2008) pp. 177–186.

[28] A. V. Korol and A. V. Solov'yov, J. Phys. B: At. Mol. Opt. Phys. **44**, 085001 (2011).

[29] Z. Chen and A. Z. Msezane, J. Phys. B: At. Mol. Opt. Phys. **45**, 235205 (2012).

[30] S. Schippers, S. Ricz, T. Buhr, A. Borovik Jr., J. Hellhund, K. Holste, K. Huber, H.-J. Schäfer, D. Schury, S. Klumpp, K. Mertens, M. Martins, R. Flesch, G. Ulrich, E. Rühl, T. Jahnke, J. Lower, D. Metz, L. P. H. Schmidt, M. Schöffler, J. B. Williams, L. Glaser, F. Scholz, J. Seltmann, J. Viefhaus, A. Dorn, A. Wolf, J. Ullrich, and A. Müller, J. Phys. B: At. Mol. Opt. Phys. **47**, 115602 (2014).

[31] A. Müller, D. Bernhardt, A. Borovik Jr., T. Buhr, J. Hellhund, K. Holste, A. L. D. Kilcoyne, S. Klumpp, M. Martins, S. Ricz, J. Viefhaus, and S. Schippers, Astrophys. J. **836**, 166 (2017).

[32] J. Viefhaus, F. Scholz, S. Deinert, L. Glaser, M. Ilchen, J. Seltmann, P. Walter, and F. Siewert, Nucl. Instrum. Methods **A710**, 151 (2013).

[33] A. M. Covington, A. Aguilar, I. R. Covington, M. F. Gharaibeh, G. Hinojosa, C. A. Shirley, R. A. Phaneuf, I. Álvarez, C. Cisneros, I. Dominguez-Lopez, M. M. Sant'Anna, A. S. Schlachter, B. M. McLaughlin, and A. Dalgarno, Phys. Rev. A **66**, 062710 (2002).

[34] A. Müller, S. Schippers, D. Esteves-Macaluso, M. Habibi, A. Aguilar, A. L. D. Kilcoyne, R. A. Phaneuf, C. P. Ballance, and B. M. McLaughlin, J. Phys. B: At. Mol. Opt. Phys. **47**, 215202 (2014).

[35] A. Müller, S. Schippers, J. Hellhund, K. Holste, A. L. D. Kilcoyne, R. A. Phaneuf, C. P. Ballance, and B. M. McLaughlin, J. Phys. B: At. Mol. Opt. Phys. **48**, 235203 (2015).

[36] B. M. McLaughlin, C. P. Ballance, S. Schippers, J. Hellhund, A. L. D. Kilcoyne, R. A. Phaneuf, and A. Müller, J. Phys. B: At. Mol. Opt. Phys. **49**, 065201 (2016).

[37] A. Müller, S. Schippers, J. Hellhund, A. L. D. Kilcoyne, R. A. Phaneuf, and B. M. McLaughlin, J. Phys. B: At. Mol. Opt. Phys. **50**, 085007 (2017).

[38] A. Müller, A. Borovik Jr., T. Buhr, J. Hellhund, K. Holste, A. L. D. Kilcoyne, S. Klumpp, M. Martins, S. Ricz, J. Viefhaus, and S. Schippers, Phys. Rev. Lett. **114**, 013002 (2015).

[39] S. Schippers, R. Beerwerth, L. Abrok, S. Bari, T. Buhr, M. Martins, S. Ricz, J. Viefhaus, S. Fritzsche, and A. Müller, Phys. Rev. A **94**, 041401(R) (2016).

[40] S. Schippers, M. Martins, R. Beerwerth, S. Bari, K. Holste, K. Schubert, J. Viefhaus, D. W. Savin, S. Fritzsche, and A. Müller, Astrophys. J. **849**, 5 (2017).

[41] A. Müller, A. Borovik Jr., T. Buhr, J. Hellhund, K. Holste, A. L. D. Kilcoyne, S. Klumpp, M. Martins, S. Ricz, J. Viefhaus, and S. Schippers, Phys. Rev. A **97**, 013409 (2018).

[42] A. Müller, A. Borovik Jr., S. Bari, T. Buhr, K. Holste, M. Martins, A. Perry-Saßmannshausen, R. A. Phaneuf, S. Reinwardt, S. Ricz, K. Schubert, and S. Schippers, Phys. Rev. Lett. **120**, 133202 (2018).

[43] A. Müller, E. Lindroth, S. Bari, A. Borovik Jr., P.-M. Hillenbrand, K. Holste, P. Indelicato, A. L. D. Kilcoyne, S. Klumpp, M. Martins, J. Viefhaus, P. Wilhelm, and S. Schippers, Phys. Rev. A **98**, 033416 (2018).

[44] B. L. Henke, E. M. Gullikson, and J. C. Davis, At. Data Nucl. Data Tables **54**, 181 (1993).

[45] M. Tronc, G. C. King, and F. H. Read, J. Phys. B: At. Mol. Opt. Phys. **12**, 137 (1979).

[46] I. Harrison and G. C. King, J. Electron Spectrosc. Relat. Phenom. **43**, 155 (1987).

[47] A. P. Hitchcock and C. E. Brion, J. Phys. B: At. Mol. Opt. Phys. **13**, 3269 (1980).

[48] F. Wuilleumier, J. Phys. Col. **32 (C4)**, 88 (1971).

[49] N. Mardirossian and M. Head-Gordon, Mol. Phys. **115**, 2315 (2017).

[50] M. W. Schmidt, K. K. Baldridge, J. A. Boatz, S. T. Elbert, M. S. Gordon, J. H. Jensen, S. Koseki, N. Matsunaga, K. A. Nguyen, S. Su, T. L. Windus, M. Dupuis, and J. A. Montgomery, J. Comput. Chem. **14**, 1347 (1993).

[51] A. A. Popov and L. Dunsch, J. Am. Chem. Soc. **129**, 11835 (2007).

[52] K. Hermann, L. G. M. Pettersson, M. E. Casida, C. Daul, A. Goursot, A. Koester, E. Proynov, A. St-Amant, and D. R. Salahub, and contributing authors: V. Carravetta, H. Duarte, C. Friedrich, N. Godbout, M. Gruber, J. Guan, C. Jamorski, M. Leboeuf, M. Leetmaa, M. Nyberg, S. Patchkovskii, L. Pedocchi, F. Sim, L. Triguero, and A. Vela, "StoBe-deMon version 3.3 (2014)," (2014).

[53] A. D. Becke, Phys. Rev. A **38**, 3098 (1988).

[54] J. P. Perdew, Phys. Rev. B **33**, 8822 (1986).

[55] N. Godbout, D. R. Salahub, J. Andzelm, and E. Wimmer, Can. J. Chem. **70**, 560 (1992).

[56] L. Triguero, L. G. M. Pettersson, and H. Ågren, J. Phys. Chem. A **102**, 10599 (1998).

[57] B. Obst, T. Richter, M. Martins, and P. Zimmermann, J. Phys. B: At. Mol. Opt. Phys. **34**, L657 (2001).

[58] K. Hirsch, V. Zamudio-Bayer, F. Ameseder, A. Langenberg, J. Rittmann, M. Vogel, T. Möller, B. Issendorff, and J. T. Lau, Phys. Rev. A **85**, 062501 (2012).

[59] R. S. Mulliken, J. Chem. Phys. **23**, 1833 (1955).

[60] P.-O. Löwdin, Phys. Rev. **97**, 1474 (1955).

[61] Z. Slanina and S. Nagase, Chem. Phys. Chem. **6**, 2060 (2005).

[62] J. S. Kaastra and R. Mewe, Astron. Astrophys. Suppl. Ser. **97**, 443 (1993).

[63] M. Krause, H. Kuzmany, P. Georgi, L. Dunsch, K. Vietze, and G. Seifert, J. Chem. Phys. **115**, 6596 (2001).

[64] L. S. Cederbaum, J. Zobeley, and F. Tarantelli, Phys. Rev. Lett. **79**, 4778 (1997).

[65] T. Jahnke, J. Phys. B: At. Mol. Opt. Phys. **48**, 082001 (2015).

[66] M. Martins, K. Godehusen, T. Richter, P. Wernet, and P. Zimmermann, J. Phys. B: At. Mol. Opt. Phys. **39**, R79 (2006).

[67] A. A. Popov and L. Dunsch, J. Am. Chem. Soc. **130**, 17726 (2008).

[68] G. B. Adams, M. O'Keeffe, and R. S. Ruoff, J. Phys. Chem. **98**, 9465 (1994).

[69] A. Rüdel, R. Hentges, U. Becker, H. S. Chakraborty, M. E. Madjet, and J. M. Rost, Phys. Rev. Lett. **89**, 125503 (2002).